# Quantum sine-Gordon simulations with superconducting circuits

Author: Adrià Riera Moral
*Facultat de Física, Universitat de Barcelona, Diagonal 645, 08028 Barcelona, Spain.*

Advisors: David López-Núñez and Sofyan Iblisdir

**Abstract:** In this work, we study how we can simulate the quantum sine-Gordon (qSG) model using superconducting quantum circuits. We describe our circuit configuration and demonstrate why it reproduces the qSG and how to simulate it. Our final result is the comparison between the simulated energy spectrum of the circuit and the lightest breather state energy, which are expected to map to each other in the continuum limit. We find a reasonable agreement between our simulations and the exact result, even though we were limited by different reasons. Finally, we propose a roadmap to improve the results.

## I. INTRODUCTION

In the context of quantum mechanics, it is common to struggle to simulate problems of a simple nature on a classical computer. Using a quantum system to investigate quantum problems seems to be a reasonable approach, since it can faithfully describe the quantum degrees of freedom. A possible method is quantum simulation, that consists on mimicking a quantum system with another that is easier to manipulate [1]. Quantum simulations are usually divided into digital and analog simulations. In the latter one, the Hamiltonian of the new system tries to be as close as possible as to the original one. There are different possible technologies to implement analog quantum simulations, for instance trapped ions, ultracold atoms or superconducting circuits [2]. In contrast to the other approaches, superconducting circuits are manufactured, hence most parameters are not given by nature but designed by humans, which provides more control over the system parameters and leads to more possibilities of optimization. On the other hand, as superconducting circuits are macroscopic systems, they are more susceptible to noise, which introduce errors on the simulations; and despite having more control on the circuit parameters, its reproducibility can still be improved. However, superconducting circuits have proven already to be one of the most promising platforms for performing quantum information science, being currently the leading platform in quantum computation [3].

Quantum field theories (QFTs) are among the most successful descriptions of the physical world, which were initially developed to unify quantum mechanics and special relativity. Carrying out exact computations using QFTs is notoriously hard. However, perturbative calculations in the form of Feynman diagrams have yielded remarkably accurate results. When a perturbative expansion is not possible, one is usually forced to use (often) heavy numerical simulations. While remarkable progress has been achieved in analyzing QFTs using numerical or effective field theory methods [4], many quantities of interest remain elusive, either due to the computational limitations or due to the lack of an effective theory.

In this work, we use the know capabilities of superconducting circuit to study QFT[5, 6]. In particular, we study a proposed [7] superconducting circuit to investigate one of the paradigmatic integrable QFT models: the quantum sine-Gordon (qSG) model in 1+1 space-time dimensions, which is of great interest because one can obtain exact analytical results even in the non-perturbative regime, which makes it an excellent toy laboratory model for more complicated QFTs. It is important to remark that, even though the investigation of this model is of great interest for a lot of Quantum Field theorists, it has never been implemented experimentally. This work represents a starting point to the study of qSG-like models using superconducting quantum simulators that may be extended in the future with actual experimental implementations.

The article is organized as follows. In Sec. II, we summarize two relevant topics in this work, superconducting circuits, and the sine-Gordon model. In Sec. III, we take a look at the circuit and the methods used in this work, from the circuit analysis to the simulation. In Sec. III D, we provide some analytical results and the identification of the first breather in our energy plot. In Sec. V, we talk about the conclusions and open the discussion for future modifications and objectives.

## II. THEORY BACKGROUND

### A. Superconducting Circuits

Superconductivity is a property of matter that is observed at low temperatures. Below a certain critical temperature, some materials become superconducting, which is characterized by two basic properties: firstly, they offer no resistance to the passage of electrical current thus allowing current to flow inside the material without energy dissipation. Secondly, they actively exclude magnetic fields from its interior, which is known as the Meissner effect. These properties were modeled successfully by the BCS theory [8].

In order to build and control superconducting circuits in the quantum regime, one relies basically on three elements: capacitors, inductors, and Josephson junctions

(JJ). The capacitor is an element that stores energy in an electric field and the inductor is a coil which stores energy in the magnetic field. The I-V characteristics for these two elements are,

$$i_C(t) = C\frac{dv}{dt},\ \ v_L(t) = \frac{d\phi}{dt} = L\frac{di}{dt}, \tag{1}$$

where $\phi = Li$ is the magnetic flux, C and L are the capacitance and inductance respectively. Both inductors and capacitors are linear. In order to control the degrees of freedom of a superconducting circuit in the quantum regime, however, nonlinear elements are needed. Josephson junction provide this nonlinearity together with being disipationless thanks to superconductivity. Josephson junctions are formed by separating two superconducting electrodes with an insulator thin enough so that the macroscopic wave function of the superconductor on each side of the barrier tunnels through it. It has been shown [8] that JJ has the I-V characteristics,

$$I = I_0\sin(\varphi),\ \ V = \frac{\Phi_0}{2\pi}\dot{\varphi}, \tag{2}$$

where $\Phi_0 = h/2e$ is the superconducting flux quantum, $I_0$ is the critical current above which the JJ becomes dissipative, $\varphi = \theta_1 - \theta_2$ and V are respectively gauge-invariant superconducting phase and voltage across the junction. A JJ also has some intrinsic capacitance that must be taken into account.

Superconducting circuits obey quantum mechanical laws, but their degrees of freedom follow the standard laws of electric circuits. The quantum description of an electrical circuit is obtained through circuit quantization. In order to do so, it is convenient to express the current flowing through each element of the circuit in terms of an associated local magnetic flux, $\Phi$. At each node, Kirchoff relation for incoming and outgoing currents can be applied as in standard circuits:

$$\sum I_{in} = \sum I_{out}. \tag{3}$$

Using Eqs. 1-2, Eq. 3 constitutes the equation of motion for each independent flux variable in the circuit. These equations can also be derived through

$$\frac{d}{dt}\left(\frac{\partial\mathcal{L}}{\partial\dot{\Phi}_i}\right) = \frac{\partial\mathcal{L}}{\partial\Phi_i}. \tag{4}$$

Then, the lagrangian of the system is obtained by integration. The conjugate moment is defined as,

$$q_i = \frac{\partial\mathcal{L}}{\partial\dot{\Phi}_i} \tag{5}$$

Finally, using the Legendre transformation

$$\mathcal{H} = \sum_i q_i\dot{\Phi}_i - \mathcal{L}, \tag{6}$$

the final Hamiltonian of our superconducting circuit is obtained. The final step towards quantizing the circuits consists on promoting the flux and charge variable to quantum mechanical operators

$$\Phi_i \longrightarrow \hat{\Phi}_i\,,\ \ q_i \longrightarrow \hat{q}_i, \tag{7}$$

which, analogously to position and momentum operators, follow the commutation relations, $\left[\hat{\Phi}_i, \hat{q}_j\right] = \delta_{ij}i\hbar$. However, through the rest of the paper, we will omit the hat for convenience, only using it in necessary derivations.

### B. Sine-Gordon model

The sine-Gordon Lagrangian is given by the action

$$S = \frac{1}{2}\int d^2x\,(\partial_\mu\phi)^2 + M_0\int d^2x\cos(\beta\phi), \tag{8}$$

where $M_0$ is the mass-parameter of the action. The excitations of any QFT are particles, and, in the qSG model, these are solitons and breathers. The breathers are soliton-antisoliton bound states. A more formal derivation of these excitations can be found in Appendix A.

Soliton mass is given by [9]

$$M = \frac{2\Gamma(\xi/2)}{\sqrt{\pi}\Gamma\left(\frac{1+\xi}{2}\right)}\left[\frac{M_0\pi\Gamma\left(1-\frac{\beta^2}{8\pi}\right)}{2\Gamma\left(\frac{\beta^2}{8\pi}\right)}\right]^{\frac{1}{2-\frac{\beta^2}{4\pi}}}, \tag{9}$$

where $\xi = \frac{\beta^2}{8\pi-\beta^2}$. Contrary to classical sine-Gordon, there are only a finite number of breather states in the quantum regime. The mass of the $n^{th}$ breather state is given by

$$m_n = 2M\sin\left(\frac{n\pi\xi}{2}\right),\ \ n = 1, 2, ..., \left\lfloor\frac{1}{\xi}\right\rfloor. \tag{10}$$

Note that the mass of the breather is always less than twice the soliton mass, as we would expect for a bound motion of a soliton-antisoliton pair. At small $\beta$ the lightest breather is $n = 1$ and its mass should coincide with the energy of the first excited state of the system [10].

## III. DEVELOPMENT SECTION

### A. Circuit

In this work we follow [7] to investigate the qSG with a certain configuration of superconducting circuit which is composed of an array of N unit cells, with N tending to infinity, as seen in FIG. 1. Two neighboring cells are separated by Josephson junctions with junction energy $E_H$ and charging energy $E_{C_H} = 2e^2/C_H$. In addition, each cell is also separated from the ground plane by a Josephson junction, with junction energy $E_V$ and charging energy $E_{C_V} = 2e^2/C_V$.

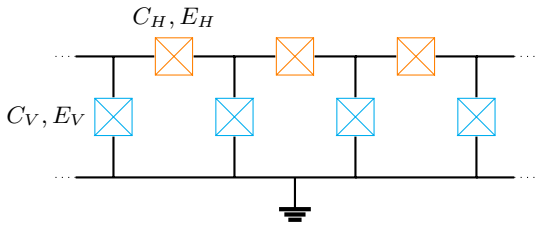


FIG. 1: Schematic of the superconducting circuit for the qSG model. Each Josephson junction is indicated by a cross with a box around it.

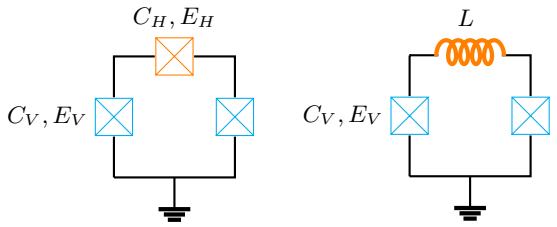


(a) Josephson junction (b) Inductance

FIG. 2: Circuit configuration used in this work (a) and future implementation (b).

There are two important cases. When $E_V = 0$, then the Josephson junctions on the vertical perform as simple capacitances. This case has been analyzed perturbatively [11] and one can see that it reproduces, in the continuum limit, the action

$$S_0 = \frac{1}{2\pi K}\int d^2x \left[\frac{1}{u}(\partial_t\varphi)^2 + u(\partial_x\varphi)^2\right], \qquad (11)$$

which is called the Luttinger Liquid action with plasmon velocity $u$ and Luttinger parameter K. These parameters in the perturbative approximation, working in the regime where $E_{C_H} \ll E_{C_V}, E_V \ll E_H$, are given by [12]

$$u \approx a\sqrt{2E_{C_V}E_H}, \quad K \approx \frac{1}{2\pi}\sqrt{\frac{2E_{C_V}}{E_H}}, \qquad (12)$$

where $a$ is the lattice spacing of the circuit. In the case of $E_V \neq 0$, there is an additional term in the action, see Sec. III C, and properly describes the qSG. This is the situation in which we are interested in.

### B. Circuit Quantization

As mentioned before, circuit quantization is a method which allows one to obtain the Lagrangian and Hamiltonian of a superconducting circuit. First, all nodes should be identified, one of them should be put as ground, and from the ground mode, all the nodes must be connected following one path, forming the spanning tree. Then following the steps described in Sec. III A, The Lagrangian and Hamiltonian can be obtained. Full derivation for the example in FIG. 2(a) can be found in Appendix B. In our case of interest [see FIG. 1], the same analysis is applied and the result Hamiltonian is given by

$$\begin{aligned} H = {} & E_{C_V}\sum_{i=1}^{L} n_i^2 + \delta E_{C_V}\sum_{i=1}^{L-1} n_i n_{i+1} \\ & - E_H\sum_{i=1}^{L-1}\cos(\varphi_i - \varphi_{i+1}) - E_V\sum_{i=1}^{L}\cos(\varphi_i), \end{aligned} \qquad (13)$$

where $n_i$ is the excess number of Cooper pairs on the $i^{th}$ island and $\delta$ is small parameter, $\delta < 1$. The third term, which appears due to the Josephson junctions in the horizontal link, can be approximated to its Taylor expansion if $E_H$ is sufficiently small, $\cos(\varphi_i - \varphi_{i+1}) \approx 1 - (\varphi_i - \varphi_{i+1})^2/2$, which is convenient for the qSF simulation. Computationally, it is easier to simulate our system using the cosine, as will be explained in Sec. IIID. However, it is experimentally possible to have a large inductance without the need of Josephson junction [see FIG. 2(b)] by using granular aluminum [13], which is a high kinetic inductance material. Then, it allow us to avoid the limitation in the regime $E_H \gg E_{C_V}$, and then this term is rewritten as: $E_L\sum_{i=1}^{L-1}(\varphi_i - \varphi_{i+1})^2$.

### C. Lagrangian to Action

In order to transition from a set of discrete generalized coordinates $q_n$, into a continuous field coordinate $\phi(x)$ we follow the steps explained in [14]. As stated in the previous section, we work in the regime of small $E_H$ and will consider $\delta = 0$ for simplicity. Then, Lagrangian can be written as a linear part $L_0$ and the interaction part, $L_{int}$, with the remaining cosinus term. By taking the continuous limit and using $S = \int dtL$ we arrive at

$$\begin{aligned} S = {} & \int d^2x \left[\frac{1}{2E_{C_V}a}(\partial_t\phi)^2 + aE_H(\partial_x\phi)^2\right] \\ & + E_V\int d^2x\cos(\phi). \end{aligned} \qquad (14)$$

Full derivation can be found in Appendix C. If we compare this final expression with Eq. (11), where $\phi = \beta\varphi$, one can easily see the connections in Eq. (12). Furthermore, the qSG coupling and the mass-parameter of the action, in units of $a = 1$, are $\beta = \sqrt{\pi K}$ and $M_0 = E_V$ respectively.

### D. Numerical Simulation

We have followed an exact diagonalization of the Hamiltonian in order to obtain the eigenenergies and eigenstates of the system. Since no inductance is considered, it is convenient to choose the charge basis as the

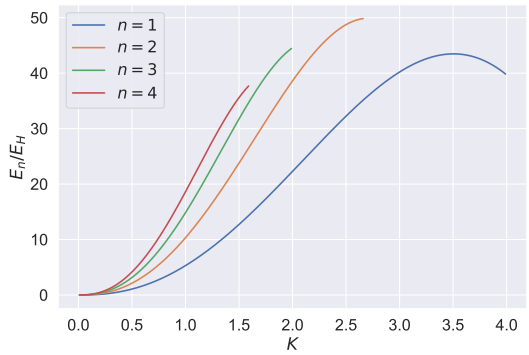


FIG. 3: Variation of $E_n$, which is the energy of the $n^{th}$ breather, and is defined as $E_n = m_n u^2$, being $m_n$ the $n^{th}$ breather mass and $u$ the plasmon velocity, with the variation of the Luttinger parameter, K. ($E_V = 0.01$)

basis in which we define our states. This is computationally convenient because the capacitive terms, which depend on $n_i^2$ and $n_i n_j$, are diagonal, and the Josepshson junction terms are represented in the upper and lower diagonals, then most elements of the matrix are zero. For computing the Josephson terms one has to note that $\cos\varphi = (e^{i\varphi} + e^{-i\varphi})/2$. Then we can use the following relation, $e^{\pm i\hat{\varphi}}|n\rangle = |n \mp 1\rangle$. So the effect of a Josephson junction terms over a charge state $|n\rangle$, is

$$\cos\hat{\varphi}|n\rangle = \frac{1}{2}(|n+1\rangle + |n-1\rangle). \tag{15}$$

In case we introduce an inductance, we would need to change our basis to the harmonic basis, composed of an inductance and capacitance, and the matrix representation of the cosine would be much more difficult to compute. One could also change the Hamiltonian representation into the phase basis and numerically integrate the Schrodinger equation, which may be convenient for linear inductors. We have kept the Josephson junctions during the simulation, however in the experiment, as mentioned before, it would be better to use an inductance [see FIG. 2(b)]. Finally, using a python library called scipy.sparse library we are able to perform an exact diagonalization, hence obtaining the energy spectrum.

## IV. RESULTS

First, we present the breathers' energy in FIG 3. We observe that for the whole range of $K$ the lightest breather corresponds to the first breather, $n = 1$, and as K increases, the heavier breathers disappear. For $K < 4$ there exist breather states because the interaction is attractive [15], thus the solitons and anitsolitons form bound states. For $K > 4$ this interaction becomes repulsive, therefore no bound states are formed. In the limit $K \to 0$, $n$ increases, recovering the classic limit where we have a continuum number of breather states.

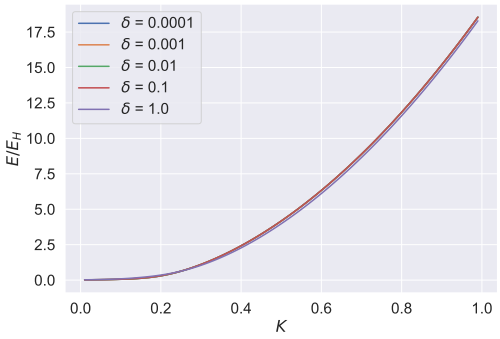


(a)

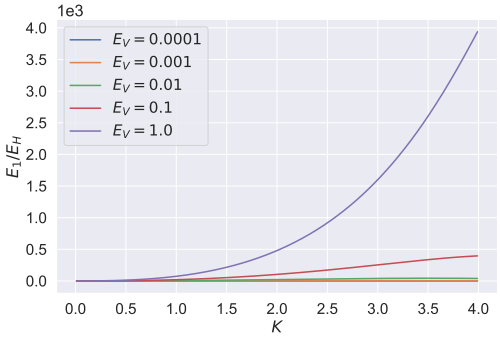


(b)

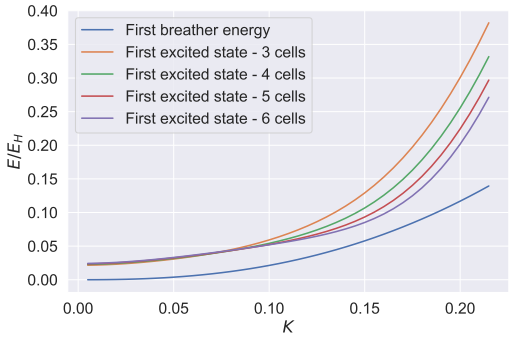


(c)

FIG. 4: (a) Variation of the energy with the variation of K, using different values for the parameter $\delta$. (b) Variation of the first breather energy with the variation of K, using different values for $E_V$. (c) Comparison between the energy spectrum of our circuit with different number of cells and the variation of the first breather energy, with the K variation.

We did some prior tests in order to check our simulations were correct. We simulated the flux qubit, and compared the energy spectrum with the results in [16]. We also checked which is the maximum number of charges needed for the solution to converge, which is an important parameter for our simulations, because the number of states is $N = (2n_{max} + 1)^L$, where L is the number of cells, and so the matrix $N \times N$, and the computational

costs scale quickly increasing $n_{max}$. As can be seen in FIG. 4(a), we show that, for small $\delta$, we can neglect its effect as simulations are unaffected by its value.

Then, we present some simulations for different $E_V$, which corresponds to different $M_0$. We have access to the full range of parameters space. However, as mentioned in Sec. III C, simulations using the Josephson Junctions instead of inductances in the horizontal link is only valid in the regime where $E_H \gg E_{C_V}$, which corresponds to $K \ll 1$.

In FIG. 4(c), we compare the results of the breather energy with our superconducting circuit model for different number of array cells, limiting the comparison to the regime of small $K$. The energy of the simulated first excited state and the energy of the first breather should map to each other. The first breather energy is considerably close taking into account that the simulations are far from the continuum limit. As we increase the number of cells, the simulation consistently approach the breather energy, which gives hope that in the limit with infinite cells it will get closer. Notice that 6 array cells is the maximum number of cells we can simulate using a conventional laptop with 2 cores and 8 GB of RAM. Discrepancy is expected as perturbative definition of $K$ and $u$ are known to be not ideal, producing an offset that could be comparable to what is seen in the simulations.

## V. CONCLUSIONS AND FUTURE WORLD

In this work, we have studied the validity of our superconducting quantum circuit configuration [see FIG. 1] of reproducing the qSG model, from the mathematical derivations to the computational simulation. We have analyzed the simplest viable experimental implementation that could be performed, which consists on measuring the first excitation of the array which should correspond to the energy of the first breather state of the qSG. Despite our results don't match perfectly with the exact solutions, this is expectable for at least two reasons: the perturbative approximation of the qSG parameters produces an offset variation [7], and the solutions correspond to the continuum limit which is far from our simulations.

Since this work is a starting point for understanding this kind of systems, we propose different improvements that can be implemented in the future. First, instead of working with the perturbative approximations, one can use the density matrix renormalization group (DMRG) technique which has been proved in [7] that improves the results. Another way of improving the results would be to perform these simulations on a bigger machine, such as the computers at PIC Port d'Informació Científica) or BSC (Barcelona Supercomputing Centre). Then, as mentioned in Sec. III B it is experimentally possible to have large inductance by using granular aluminum, so, changing the horizontal Josephson junctions for an inductance will allow to get better results with higher $K$. as we will not be restricted to $K \ll 1$. Finally, this work is intended to be continued with an experimental realization that could overcome most of the issues faced during the simulations. Large arrays of junctions have already been successfully implemented and granular aluminum has shown to provide the large inductances needed in this work. Then, fabricating an array with the proper design parameters should allow testing the results in a limit much closer to the continuum and without the limitation of using junctions in the horizontal array.

### Acknowledgments

I would like to express my gratitude to David López-Núñez for his high involvement, guidance, and help through this project. I would also like to thank Jan Ollé Aguilera, who has been collaborating on this project and has helped a lot.

[1] Richard P. Feynman, International Journal of Theoretical Physics 21 (1982).
[2] Samuel A. Wilkinson, Michael J. Hartmann, Appl. Phys. Lett. 116, 230501 (2020).
[3] Frank Arute, Kunal Arya, John M. Martinis, Nature 574 (2019).
[4] Aoyama, T. et al. Phys. Rep. 887 (2020).
[5] Ananda Roy, Hubert Saleur, Phys. Rev. B 100, 155425 (2019).
[6] Fernando Quijandría, Juan José García-Ripoll, David Zueco, Phys. Rev. B 90, 235142 (2014)
[7] Ananda Roy, Dirk Schuricht, Johannes Hauschil, Frank Pollmann, Hubert Saleur, Nucl. Phys. B 968, 115445 (2021).
[8] Michael Tinkham, Introduction to superconductivity (1996).
[9] A. B. Zamolodchikov, International Journal of Modern Physics A 10 (08) (1995).
[10] Sidney Coleman, Aspects of symmetry: Selected Erice lectures of Sydney Coleman (1985).
[11] L. I. Glazman, A. I. Larkin, Phys. Rev. Lett. 79 (1997).
[12] M. Goldstein, M. H. Devoret, M. Houzet, L. I. Glazman, Phys. Rev. Lett. 110 (2013).
[13] Lukas Grünhaupt, Martin Spiecker, Daria Gusenkova, Nataliya Maleeva, Sebastian T. Skacel, Ivan Takmakov, Francesco Valenti, Patrick Winkel, Hannes Rotzinger, Wolfgang Wernsdorfer, Nature Materials 18 (2019)
[14] Hugo Laurell, A summary on Solitons in Quantum field theory (2016).
[15] Tanmay Vachaspati, Kinks and Domain Walls: An Introduction to Classical and Quantum Solitons (2006).
[16] T. P. Orlando, J. E. Mooij, Lin Tian, Caspar H. van der Wal, L. Levitov, Seth Lloyd, J. J. Mazo, Physical Review B 60:15398 (1999).

### Appendix A: Quantum Sine-Gordon excitations

The sine-Gordon Lagrangian is given by [15]

$$\mathcal{L} = \frac{1}{2}(\partial_\mu \phi)^2 - \frac{\alpha}{\beta^2}(1 - \cos\beta\phi). \tag{A1}$$

In 1+1 spacetime dimensions, the field $\phi$ is dimensionless, $\beta$ is also dimensionless and $\alpha$ has units of mass squared. For Lagrangians with a single scalar field, the (classical) equation of motion is given by the Euler-Lagrange equation

$$\partial_\mu \left( \frac{\partial \mathcal{L}}{\partial(\partial_\mu \phi)} \right) = \frac{\partial L}{\partial \phi}. \tag{A2}$$

In our case, $\frac{\partial \mathcal{L}}{\partial(\partial_\mu \phi)} = \partial^\mu \phi$ and $\frac{\partial L}{\partial \phi} = -\frac{\alpha}{\beta}\sin(\beta\phi)$, so we have the equation

$$\partial_\mu \partial^\mu \phi + \frac{\alpha}{\beta}\sin(\beta\phi) = 0, \tag{A3}$$

where $\partial_\mu \partial^\mu \phi = \partial_t^2 \phi - \partial_x^2 \phi$. Kinks and breathers are solutions to this equation of motion. The kink and antikink solutions are given by [15]

$$\phi_k = \frac{4}{\beta}\tan^{-1}(e^{\sqrt{\alpha}x}) \tag{A4}$$

$$\overline{\phi}_k = \frac{4}{\beta}\tan^{-1}(e^{-\sqrt{\alpha}x}) \tag{A5}$$

Breathers are bound states of a soliton and an antisoliton:

$$\phi_b(t,x) = \frac{4}{\beta}\tan^{-1}\left[\frac{\eta\sin(wt)}{\cosh(\eta w x)}\right], \tag{A6}$$

where $\eta = \sqrt{\alpha - w^2}/w$ and $\omega$ is a continuos parameter $0 < w < \sqrt{\alpha}$.

### Appendix B: Circuit quantization

Following the steps described in Sec. IIIB, we do the exact circuit quantization for FIG. 5.

1. First, all the nodes should be identified. Then, one of them should be set as ground. This is the same as choosing a zero in the energy or in a coordinate system. An arbitrary direction of the current in every branch has to be chosen and one has to be consisten with that choice.

2. We must obtain two movement equations for each of the two actives nodes: A and B. We will use the Kirchhoff law $\sum I_{in} = \sum I_{out}$ and the relations of the current for the JJ:

Node A:

$$\sum I_{in} = C_V(\ddot{\phi}_A - \ddot{\phi}_G) + I_V \sin(\frac{2\pi}{\Phi_0}(\phi_A - \phi_G)) \tag{B1}$$

$$\sum I_{out} = C_H(\ddot{\phi}_B - \ddot{\phi}_A) + I_H \sin(\frac{2\pi}{\Phi_0}(\phi_B - \phi_A)) \tag{B2}$$

Where we have defined $\ddot{\phi}_G = \phi_G = 0$. Now, matching both equations, we reorganize the terms as follows:

$$\begin{aligned}\ddot{\phi}_A(C_V + C_H) - \ddot{\phi}_B C_H =& I_H \sin(\frac{2_1}{\Phi_0}(\phi_B - \phi_A)) \\ &- I_V \sin(\frac{2\pi}{\Phi_0}\phi_A)\end{aligned} \tag{B3}$$

Node B:

$$\sum I_{in} = C_H(\ddot{\phi}_B - \ddot{\phi}_A) + I_H \sin(\frac{2\pi}{\Phi_0}(\phi_B - \phi_A)) \tag{B4}$$

$$\sum I_{out} = C_V(\ddot{\phi}_G - \ddot{\phi}_B) + I_V \sin(\frac{2\pi}{\Phi_0}(\phi_G - \phi_B)) \tag{B5}$$

Combining both and reorganizing the terms we arrive to the movement equation for node B:

$$\begin{aligned}-C_H\ddot{\phi}_A + \ddot{\phi}_B(C_H + C_V) =& - I_V \sin(\frac{2\pi}{\Phi_0}\phi_B) \\ &- I_H \sin(\frac{2\pi}{\Phi_0}(\phi_B - \phi_A))\end{aligned} \tag{B6}$$

3. The next step is finding the Lagrangian integrating the two movement equations, knowing that

$$\frac{d}{dt}\left(\frac{\partial \mathcal{L}}{\partial \dot{\Phi}_i}\right) = \frac{\partial \mathcal{L}}{\partial \Phi_i} \tag{B7}$$

Then we will obtain the dependence of the Lagrangian on each of the variables. Integrating equation (B3) on both sides, we obtain

$$\begin{aligned}\mathcal{L}_A =& \frac{\dot{\phi}_A^2}{2}(C_V + C_H) - \dot{\phi}_B\dot{\phi}_A C_H \\ &+ E_H \cos(\frac{2\pi}{\Phi_0}(\phi_B - \phi_A)) + E_V \cos(\frac{2\pi}{\Phi_0}\phi_A)\end{aligned} \tag{B8}$$

Using now equation (B6)

$$\begin{aligned}\mathcal{L}_B =& - \dot{\phi}_A\dot{\phi}_B C_H + \frac{\dot{\phi}_B^2}{2}(C_V + C_H) \\ &+ E_V \cos(\frac{2\pi}{\Phi_0}\phi_B) + E_H \cos(\frac{2\pi}{\Phi_0}(\phi_B - \phi_A))\end{aligned} \tag{B9}$$

Combining all terms the total Lagrangian results in

$$\begin{aligned}\mathcal{L} =& \frac{C_V + C_H}{2}(\dot{\phi}_A^2 + \dot{\phi}_B^2) - 2C_H \dot{phi}_A\dot{\phi}_B \\ &+ E_V[\cos(\frac{2\pi}{\Phi_0}\phi_A) + \cos(\frac{2\pi}{\Phi_0}\phi_B)] \\ &+ 2E_H \cos(\frac{2\pi}{\Phi_0}(\phi_B - \phi_A))\end{aligned} \tag{B10}$$

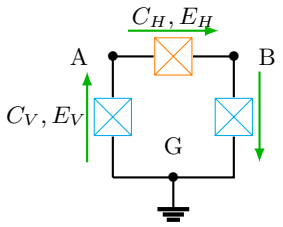


FIG. 5: 3 Josephson junction circuit, with nodes identified and the direction of the current for each branch chosen.

It is more useful to write it in terms of the phase variable instead of charge variable, $\varphi_i = \frac{2\pi}{\Phi_0}\phi_i$.

$$\begin{aligned}\mathcal{L} =& \frac{C_V + C_H}{2}\left(\frac{\Phi_0}{2\pi}\right)^2(\dot{\varphi}_A^2 + \dot{\varphi}_B^2) \\ &- 2C_H\left(\frac{\Phi_0}{2\pi}\right)^2\dot{\varphi}_A\dot{\varphi_B} \\ &+ E_V[\cos(\varphi_A) + \cos(\varphi_B)] \\ &+ 2E_H\cos(\varphi_B - \varphi_A))\end{aligned} \tag{B11}$$

There is even another convenient mass definition:

$$\begin{aligned}m_A = m_B &= (C_V + C_H)\left(\frac{\Phi_0}{2\pi}\right)^2 \\ m_C &= 2C_H\left(\frac{\Phi_0}{2\pi}\right)^2\end{aligned} \tag{B12}$$

With all these new definitions one arrives at the following expression of the Lagrangian

$$\begin{aligned}\mathcal{L} =& \frac{1}{2}m_A(\dot{\varphi}_A^2 + \dot{\varphi}_B^2) - m_C\dot{\varphi}_A\dot{\varphi}_B \\ &+ E_V[\cos(\varphi_A) + \cos(\varphi_B)] \\ &+ 2E_H\cos(\varphi_B - \varphi_A))\end{aligned} \tag{B13}$$

The generalized momentum, $p_i = \frac{\partial\mathcal{L}}{\partial\dot{\varphi}_i}$, is now easier to compute and one find the following matrix relation

$$\begin{pmatrix}p_A \\ p_B\end{pmatrix} = \begin{pmatrix}m_A & m_C \\ -m_C & m_A\end{pmatrix}\begin{pmatrix}\dot{\varphi}_A \\ \dot{\varphi}_B\end{pmatrix} = M\begin{pmatrix}\dot{\varphi}_A \\ \dot{\varphi}_B\end{pmatrix} \tag{B14}$$

4. The final step is finding the Hamiltonian using the Legendre transformation, $\mathcal{H} = \sum_i p_i\dot{\varphi}_i - \mathcal{L}$ which can be written as:

$$\mathcal{H} = \frac{1}{2}\overrightarrow{p}^T M^{-1}\overrightarrow{p} + \mathcal{U} \tag{B15}$$

Thanks to python library simpy, one can get the exact expression of the Hamiltonian

$$\begin{aligned}\mathcal{H} =& \left(\frac{2\pi}{\Phi_0}\right)^2\frac{C_V + C_H}{C_V^2 + 2C_VC_H - 3C_H^2)}(p_A^2 + p_B^2) \\ &+ \left(\frac{2\pi}{\Phi_0}\right)^2\frac{2C_H}{C_V^2 + 2C_VC_H - 3C_H^2)}p_Ap_B \\ &- E_V[\cos(\varphi_A) + \cos(\varphi_B)] \\ &- 2E_H\cos(\varphi_B - \varphi_A))\end{aligned} \tag{B16}$$

In the regime we are working, $C_{VH}$, and using the relationS $n_i = \frac{2\pi}{\Phi_0}\frac{p_i}{2e}$, $E_{C_V} = \frac{2e^2}{C_V}$ and $\delta = \frac{4C_H}{C_V}$ we can define the Hamiltonian

$$\begin{aligned}\mathcal{H} =& E_{C_V}(n_A^2 + n_B^2) + \delta E_{C_V}n_An_B \\ &- E_V[\cos(\varphi_A) + \cos(\varphi_B)] \\ &- 2E_H\cos(\varphi_B - \varphi_A))\end{aligned} \tag{B17}$$

If we extend this calculation to a N-array system, then, the Hamiltonian describing the array is given by:

$$\begin{aligned}H_{array} =& E_{C_V}\sum_{i=1}^{L}n_i^2 + \delta E_{C_V}\sum_{i=1}^{L-1}n_in_{i+1} \\ & E_H\sum_{i=1}^{L-1}\cos(\varphi_i - \varphi_{i+1}) - E_V\sum_{i=1}^{L}\cos\varphi_i\end{aligned} \tag{B18}$$

The last step is to promote the operators to quantum mechanical operators,

$$\varphi_i \longrightarrow \hat{\varphi}_i\,,\ \ n_i \longrightarrow \hat{n}_i. \tag{B19}$$

## Appendix C: Quantum sine-Gordon lagrangian to action transformation

1. We work in the regime where $E_{HC_V}$, so, we rewrite the Lagrangian with the approximations mentioned in Sec. IIIB and assume $\delta = 0$ for simplicity, we have $L = L_0 + L_{int}$, where

$$\begin{aligned}L_0 =& \frac{1}{2E_{C_V}}\sum_{i=1}^{L}a\frac{\dot{\varphi_i}^2}{a} \\ &+ E_H\sum_{i=1}^{L-1}a^2\left(\frac{\varphi_i - \varphi_{i+1}}{a}\right)^2 \\ L_{int} =& E_V\sum_{i=1}^{L}cos(\varphi_i).\end{aligned} \tag{C1}$$

2. We apply the following limits which describes how the relevant quantities change as the separation between the equally spaced coordinates go to zero and

the discret system becomes continuos:

$$\begin{aligned} &\lim_{a\to 0}\left(\sum_{i=1}^{L} a\right) = \int dx \\ &\lim_{a\to 0} q_n = \Phi(x) \\ &\lim_{a\to 0}\left(\frac{q_i - q_{i-1}}{a}\right) = \frac{\partial \Phi}{\partial x}. \end{aligned} \tag{C2}$$

3. The Euclidean action of our system is given by $S = S_0 + S_{int}$, where

$$\begin{aligned} S_0 &= \int dt L_0 \\ &= \int d^2x \left[\frac{1}{2E_{C_V} a}(\partial_t \Phi)^2 + a E_H (\partial_x \Phi)^2\right] \\ S_{int} &= E_V \int d^2x cos(\Phi). \end{aligned} \tag{C3}$$